

Two-step flux penetration in DyMo_6S_8 antiferromagnetic superconductor

T. Krzysztan and K. Rogacki

Institute of Low Temperature and Structure Research,
Polish Academy of Sciences, 50-950 Wrocław, P.O. Box 1410, Poland

The influence of antiferromagnetic order on the mixed state of a superconductor may result in the creation of spin- \uparrow domains along the vortices. This may happen when an external magnetic field is strong enough to flip over magnetic moments in the vortex core from their ground state configuration. The formation of the domain structure is accompanied by modification of the surface energy barrier and creation of a new state, resembling Meissner state, with magnetic flux density independent on the applied field. The modified surface energy barrier has been calculated for parameters of the antiferromagnetic superconductor DyMo_6S_8 . The prediction of two-step flux penetration process has been verified by precise magnetization measurements performed on a single crystal of DyMo_6S_8 at millikelvin temperatures. A characteristic plateau on the virgin curve $B(H_0)$ has been found and attributed to the modified surface energy barrier. The end of the plateau determines a critical field, which we call the second critical field for flux penetration.

PACS numbers: 74.70.Dd, 74.60.Ec, 74.25.Ha

INTRODUCTION

Magnetism and superconductivity are two very different, competing, cooperative phenomena that are unlikely to be present simultaneously within the same sample. However, the discoveries of ternary Rare Earth (RE) Chevrel Phases REMo_6S_8 ¹ and RERh_4B_4 compounds with regular distribution of localized magnetic moments of RE atoms contradict the above statement. These materials exhibit the coexistence of various types of magnetism with superconductivity. Intensive experimental and theoretical works have shown that 4f electrons of RE atoms responsible for magnetism and 4d electrons of molybdenum chalcogenide or rhodium boride clusters responsible for superconductivity are spatially separated and thus their interaction is weak. It seems that in many of these systems superconductivity coexists rather easily with antiferromagnetic order, where usually the Neel temperature T_N is lower than the critical temperature for superconductivity T_c . On the other hand, ferromagnetism and superconductivity cannot coexist in bulk samples with realistic parameters. Quite often the ferromagnetic order is transformed into a spiral or domain-like structure, depending on the type and strength of magnetic anisotropy in the system.^{2,3} For almost two decades the problem of the interaction between magnetism and superconductivity has been overshadowed by high temperature superconductivity found in copper oxides. However, the recent discovery of the presence of magnetic order in Ru-based superconductors^{4,5,6,7,8,9} has triggered a new series of experiments and inspired a return to the so-called coexistence phenomenon.¹⁰ Most recently, the interplay between magnetism and superconductivity was studied in d-electron UGe_2 ¹¹ and ZrZn_2 ,¹² where itinerant ferromagnetism may coexist with superconductivity, and in heavy fermion UPd_2Al_3 ,¹³ where magnetic excitons are present in superconducting phase.

Among classical magnetic superconductors, the Chevrel phases have been studied most intensively.

These compounds are mainly polycrystalline materials. However, some specific features can be measured only on single crystals. One such effect is a two-step flux penetration process, predicted in Ref. (14,15) and later observed in an antiferromagnetic superconductor (oct) ErRh_4B_4 ¹⁷ and recently in DyMo_6S_8 .¹⁸ This anomaly was explained as a result of the magnetic transition taking place in the vortex core. This transition seems to create a new type of vortices with the unique magnetic structure as shown in Fig.1. In the present paper the two-step flux penetration process is calculated and analyzed for a single crystal of DyMo_6S_8 . The results are quantitatively compared with the recent experiment.¹⁸

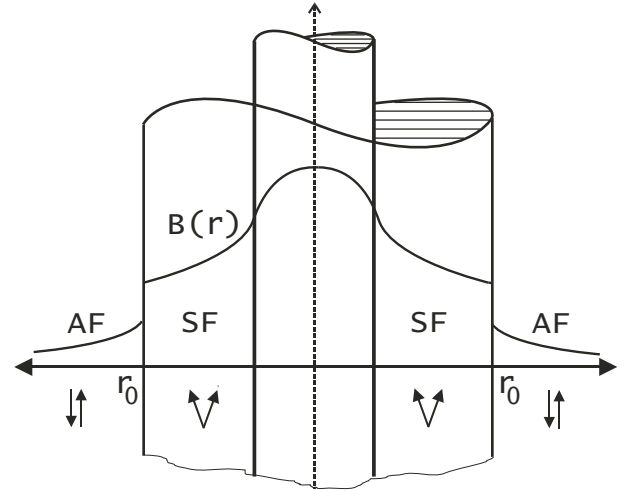


FIG. 1: The magnetic structure of the isolated vortex and the distribution of the magnetic induction around the vortex core in the spin- \uparrow SF and antiferromagnetic AF phases^{14,16}.

The DyMo_6S_8 compound with $T_c = 1.6$ K exhibits transition from the paramagnetic to the antiferromagnetic state at $T_N = 0.4$ K. Its crystal structure can be described as interconnected Mo_6S_8 units and Dy ions.

One such unit is a slightly deformed cube where S atoms sit at the corners and Mo atoms are situated at the cube-faces. The Mo_6S_8 units are arranged in a simple rhombohedral lattice and Dy ions are located in the center of the unit cell. The magnetic moments of Dy ions form a simple structure consisting of (100) planes with moments of $8:7 \mu_B$ alternately parallel and antiparallel to the [111] rhombohedral axis.

Neutron experiments performed on DyMo_6S_8 in an applied magnetic field at $T = 0.2 \text{ K}$ have revealed in the intensity spectrum a number of peaks characteristic for ferromagnetic order.¹⁹ These peaks begin to develop at $H_0 = 200 \text{ Oe}$, much below the superconducting upper critical field H_{c2} . Thus, in DyMo_6S_8 a kind of ferromagnetic order coexists with superconductivity in the same manner as antiferromagnetism. For a field applied parallel to the [111] direction (magnetic easy-axis direction), the ferromagnetic order is a spin-*op* type.²⁰ This feature is easy to understand. Consider the wellknown phase diagram of a two-sublattice antiferromagnet. An infinitesimal magnetic field applied perpendicular to the easy axis makes the ground antiferromagnetic configuration unstable against the phase transformation to the canted phase. On the contrary, if the magnetic field is applied parallel to the easy axis the antiferromagnetic (AF) phase is stable up to the thermodynamic critical field H_T . When the field is further increased, a spin-*op* (SF) phase develops in the system. Let us assume that in the antiferromagnetic superconductor the lower critical field fulfills the relation $H_{c1} < \frac{1}{2}H_T$ and that the external field H_0 is applied parallel to the easy axis. When $H_{c1} < H_0 < \frac{1}{2}H_T$ the vortices appear entirely in the AF phase. When H_0 is increased beyond $\frac{1}{2}H_T$ the phase transition to the SF phase originates in the core, because near H_{c1} the field intensity in the core is approximately twice H_{c1} .²¹ The spatial distribution of the field across the vortex is a function decreasing from the center as seen in Fig.1. Thus, the magnetic field intensity outside the core is less than H_T and, therefore, the rest of the vortex remains in the AF phase. The radius of a spin-*op* domain grows as the field is increased. The formation of domains inside the vortices should be accompanied by the creation of a new surface energy barrier¹⁵ in a new Meissner-like state in which magnetic flux density is independent on the applied field. In order to kill this state the external field should be increased above certain second critical field for flux penetration. Then, the vortices penetrating the sample will have the spin-*op* domains created along the cores. The goal of our work is to compare the model calculations based on the method of images²² with the experimental results obtained for the DyMo_6S_8 single crystal.

THEORETICAL CONSIDERATIONS

In order to describe thermodynamic behavior of DyMo_6S_8 for constant temperature and constant exter-

nal magnetic field we introduce the following free energy functional

$$F = \int dV [f_s + f_M + \frac{1}{8}(B - 4M)^2 g]. \quad (1)$$

Here B is the magnetic induction, $M = M_1 + M_2$ the magnetization of two sublattices antiferromagnetic and $H = B - 4M$ the intensity of the thermodynamic magnetic field. The free energy density of the superconducting subsystem f_s is expressed in a standard way

$$f_s = \frac{h^2}{2m} |\nabla \psi|^2 + \frac{2ie}{\hbar c} \mathbf{A} \cdot \mathbf{j} + a |\psi|^2 + \frac{1}{2} b |\psi|^4. \quad (2)$$

The quantity e/m ; $\hbar c$ denote charge and mass of the electron and light velocity, respectively. According to experiments the antiferromagnetic order is practically unaffected by the appearance of superconductivity, then it is reasonable to neglect the effect of superconductivity on the exchange interaction in F . This means that both order parameters ψ and M are coupled via the vector potential \mathbf{A} :

$$\begin{aligned} \nabla \times \mathbf{A} &= \mathbf{B} = \mathbf{H} + 4\mathbf{M} \\ \mathbf{j}_s &= \frac{c}{4} \nabla \times \mathbf{A} - \mathbf{H}, \end{aligned} \quad (3)$$

where \mathbf{j}_s denotes a superconducting current. The antiferromagnetic free energy density, which mimics the experimental results in DyMo_6S_8 , is given by the following expression

$$f_M = JM_1 \cdot M_2 + K \sum_{i=1}^2 (M_i^z)^2 + \frac{1}{2} \sum_{i=1}^2 \sum_{j=x,y,z} (\nabla_i M_j)^2. \quad (4)$$

Here J is the exchange constant between two antiferromagnetic sublattices, K denotes single ion anisotropy constant, and λ is the magnetic stiffness length. Since in the following we analyze the phenomena with characteristic length-scales much larger than the interatomic Dy-Dy distance it is justified to omit the gradient term in f_M . The components of the total magnetization vector $M = M_1 + M_2$; $M_i = M_0$ ($i = 1, 2$) have the following form in both sublattices: $M_{ix} = M_0 \sin \theta_i$; $M_{iy} = 0$; $M_{iz} = M_0 \cos \theta_i$, where θ_i (canted spin angle) is the angle between the magnetization in the sublattice and the external magnetic field directed along z -axis. The AF ($\theta_1 = 0$; $\theta_2 = \pi$) and SF phases ($\theta_1 = \theta_2 = \theta$) are in thermodynamic equilibrium in an applied field equal to the thermodynamic critical field²³

$$H_T = M_0 [K(J - K)]^{1/2}. \quad (5)$$

The canted spin angle of the SF phase is then expressed as

$$\cos \theta = \frac{KM_0}{H_T}. \quad (6)$$

The equilibrium conditions of the whole system can be obtained via minimization the Gibbs free energy functional $G = F - \frac{1}{4} \int (B - H)^2 dV$ with respect to A and M . Performing this task in the London approximation one can obtain

$$B - 4M + \frac{2}{\lambda^2} r - r (B - 4M) = 0, \quad (7)$$

where λ is the London penetration depth. The appropriate equations describing spatial distribution of M should accompany Eq.(7). To make the problem simpler we sup-

pose that the magnetization is constant across the SF domain. In this way the distribution of the magnetization around a single vortex is the following

$$M = \begin{cases} M_0 & \text{if } r \leq r_0 \\ 0 & \text{if } r > r_0 \end{cases}, \quad (8)$$

where r_0 is the radius of the spin-op domain. With the help of Eq.(7) one can write Eq.(1) for a single vortex as follows

$$F = \frac{1}{8} \int_{SF} (b_{SF} - 4M)^2 + \frac{1}{2} \int_{AF} (b_{AF} - 4M)^2 dV_{SF} + \frac{1}{8} \int_{AF} b_{AF}^2 + \frac{1}{2} \int_{AF} (r - b_{AF})^2 dV_{AF}. \quad (9)$$

Here b_{AF} and b_{SF} denote magnetic induction in AF and SF phases of a single vortex, respectively. The integrals are performed over the volume of each phase with the exclusion of the volume of the vortex core. Equation (7), for a single vortex, can be solved in the cylindrical coordinates in terms of the modified Bessel functions K_0 and I_0 :

$$\begin{aligned} b_{SF} &= C_1 K_0 \frac{r}{r_0} + C_2 I_0 \frac{r}{r_0}, \text{ for } r < r_0 \\ b_{AF} &= C_3 K_0 \frac{r}{r_0}, \text{ for } r > r_0, \end{aligned} \quad (10)$$

(λ denotes the coherence length) with the following boundary conditions:

$$\begin{aligned} b_{SF} \frac{r_0}{\lambda} &= H_T + 4M = B_T \\ b_{AF} \frac{r_0}{\lambda} &= H_T. \end{aligned} \quad (11)$$

These conditions, together with the flux quantization condition, are used to calculate the arbitrary constants in Eq.(10).

$$\begin{aligned} C_1 &= \frac{B_T \frac{r_0}{\lambda} I_1 \frac{r_0}{\lambda} - H_T \frac{r_0}{\lambda} \frac{K_1 \frac{r_0}{\lambda}}{K_0 \frac{r_0}{\lambda}} - \frac{r_0^2}{2} I_0 \frac{r_0}{\lambda}}{\frac{r_0}{\lambda} K_1 \frac{r_0}{\lambda} - I_0 \frac{r_0}{\lambda} - \frac{r_0}{\lambda} \frac{r_0}{\lambda} + \frac{r_0}{\lambda} K_0 \frac{r_0}{\lambda} - I_1 \frac{r_0}{\lambda}} \\ C_2 &= \frac{B_T \frac{r_0}{\lambda} K_1 \frac{r_0}{\lambda} - H_T \frac{r_0}{\lambda} \frac{K_1 \frac{r_0}{\lambda}}{K_0 \frac{r_0}{\lambda}} - \frac{r_0^2}{2} K_0 \frac{r_0}{\lambda}}{\frac{r_0}{\lambda} K_1 \frac{r_0}{\lambda} - I_0 \frac{r_0}{\lambda} - \frac{r_0}{\lambda} \frac{r_0}{\lambda} + \frac{r_0}{\lambda} K_0 \frac{r_0}{\lambda} - I_1 \frac{r_0}{\lambda}} \\ C_3 &= \frac{H_T}{K_0 \frac{r_0}{\lambda}}. \end{aligned} \quad (12)$$

Finally, the minimum of the Gibbs free energy of the vortex per unit length

$$F_1 = \frac{1}{8} \int_0^{r_0} dr \left[b_{SF}^2 - 4M^2 + \frac{1}{2} (r - b_{AF})^2 \right]$$

$$+ \frac{\mu_0^2 I^2}{8} \int_{r_0}^{r_L} dr \left[b_{AF} \frac{r - r_L}{r} - b_{AF} \frac{r - r_L}{r} \right], \quad (13)$$

with respect to r_0 determines:

$$\frac{r_0}{\mu_0} = \frac{0}{2B_T}. \quad (14)$$

The integrals in Eq.(13) are performed over the cylindrical element of the surface of the unit length along the axis of the vortex, r_1 denotes the surface of the vortex core, r_2 the surface of the SF domain, and r_L is the position of the center of the vortex in the cylindrical coordinates.

In order to study the conditions under which magnetic flux density in the sample becomes unstable in the applied magnetic field one must take into account the surface energy barrier preventing vortices from entering or exiting the sample. The presence of a surface of the superconductor leads to the distortion of the field and current of any vortex located within a distance of the order of penetration depth from the surface. The requirement that the currents cannot flow across the surface of the superconductor leads to the introduction of an image vortex, at $x = -x_L$, with vorticity opposite to the real one. Both vortices interact as real ones except that the inter-

action is attractive.

We consider semi-infinite specimen in the half space $x \geq 0$, the vortex and the external magnetic field running parallel to the surface. In the low flux density regime $\mu_0^2 < \mu_0^2 = B^2$, Clem²² has shown the existence of a vortex-free region of the width x_{vf} near the surface of the sample and constant vortex density region for $x > x_{vf}$. Within vortex-free area one can introduce locally averaged magnetic field B_M exponentially decreasing from its surface value H_0 to its average interior value B ,

$$B_M = B \cosh \frac{x - x_{vf}}{\lambda}. \quad (15)$$

The boundary condition $B_M(0) = H_0$ determines the thickness of the vortex-free region

$$x_{vf} = \lambda \cosh^{-1} \frac{H_0}{B}. \quad (16)$$

Now we can characterize the distribution of the magnetic induction around a single vortex in the vortex-free region

$$\begin{aligned} B_{SF} &= b_{SF} \frac{x - x_L}{r} - b_{AF} \frac{x + x_L}{r} + B_M \frac{x - x_{vf}}{r} \\ B_{AF} &= b_{AF} \frac{x - x_L}{r} - b_{AF} \frac{x + x_L}{r} + B_M \frac{x - x_{vf}}{r}. \end{aligned} \quad (17)$$

The Gibbs free energy of the system can now be written in the following way

$$\begin{aligned} G &= \frac{\mu_0^2 I^2}{8} \int_{r_1}^{r_2} dr \left[B_{SF} \frac{x - x_L}{r} - 2H_0 - 4M - r B_{SF} \frac{x - x_L}{r} \right. \\ &+ \frac{\mu_0^2 I^2}{8} \int_{r_1}^{r_2} dr \left[B_{AF} \frac{x - x_L}{r} - 2H_0 - r B_{AF} \frac{x - x_L}{r} \right. \\ &+ \left. \frac{\mu_0^2 I^2}{8} \int_{r_3}^{r_2} dr \left[B_{AF} \frac{x - x_L}{r} - 2H_0 - r B_{AF} \frac{x - x_L}{r} \right] \right], \end{aligned} \quad (18)$$

where r_3 is the surface of the specimen. After some transformations,^{15,22} one can obtain the Gibbs free energy per

unit length G in the following form :

$$G = \mu_0^2 I^2 \left[\frac{1}{4} D_1 b_{AF} \frac{2x_L}{r} - \frac{1}{2} D_1 H_0 - D_2 B_M \frac{x - x_{vf}}{r} \right], \quad (19)$$

where

$$\begin{aligned}
 D_1 &= \frac{db_{SF} \frac{x}{x_L}}{dx} \bigg|_{x=x_L} + \frac{db_{SF} \frac{x}{x_L}}{dx} \bigg|_{x=x_L+r_0} + \frac{db_{AF} \frac{x}{x_L}}{dx} \bigg|_{x=x_L+r_0} \\
 D_2 &= \frac{db_{SF} \frac{x}{x_L}}{dx} \bigg|_{x=x_L} + \frac{db_{SF} \frac{x}{x_L}}{dx} \bigg|_{x=x_L+r_0} + 2 \frac{db_{AF} \frac{x}{x_L}}{dx} \bigg|_{x=x_L+r_0} .
 \end{aligned}$$

G has its maximum at $x = x_{max}$ somewhere in the vortex-free region $r_0 < x_{max} < x_{vf}$. We can find x_{max} solving the force balance equation. When the external field reaches

$$H_{en2}(B) = B \cosh \frac{x_{en}}{x_L}, \quad (20)$$

where x_{en} is the vortex-free width corresponding to an external field equal to H_{en2} , the energy barrier moves within a distance r_0 of the surface ($x_0 = x_{vf}$). Thus, one can get

$$\frac{D_1}{2D_2} \frac{db_{AF} \frac{2x_L}{dx_L}}{dx_L} = B \sinh \frac{x_{en}}{x_L}. \quad (21)$$

The left hand side of the above equation gives $H_{en2}(0)$. This field may be thought as the second critical field for flux penetration calculated in the single vortex approximation.¹⁵

$$H_{en2}(0) = \frac{H_T}{\frac{r_0}{2B_T} \ln \frac{2B_T}{r_0}}. \quad (22)$$

Taking into account that $r_0 = x_{en}$ we finally obtain

$$H_{en2}(B) = \frac{q}{B^2 + H_{en2}^2(0)}. \quad (23)$$

Let us make a short summary of the calculations. When the SF phase develops inside the core of the vortex, the screening current must redistribute its flow around the vortex in order to keep the flux carried constant (flux quantum). This one can easily deduce from Eqs (10)-(12). The redistribution of the screening current causes the change in the surface energy barrier preventing vortices from entering into the sample. This is expressed in Eq.(19). It means that the density of vortices n is kept constant. Consequently the averaged flux density in the sample $B = n\phi_0$ remains constant when the external field is increased. The vortices start to penetrate into the sample again when the second critical field for flux penetration, calculated in Eq.(23), is reached.

EXPERIMENTAL DETAILS

The single crystals of $DyMo_6S_8$ were grown using the slow cooling of a melted charge closed in hermetically sealed molybdenum ampoules. Details of the crystal growth procedure are described elsewhere.^{18,24} The crystals were pure, homogeneous and large enough to be used for studying some subtle effects accompanying the magnetization process at millikelvin temperatures. Chemical composition and crystal uniformity were examined using a Hitachi Scanning Electron Microscope equipped with an energy dispersive x-ray analyzer. Single-crystal x-ray diffraction measurements were performed at room temperature on a Siemens SMART CCD diffractometer. The electron probe microanalysis of the regular-shaped crystals showed a composition corresponding to the $DyMo_6S_8$ formula. The cell parameters in the rhombohedral lattice were $a_R = 6.452 \times 10^8$ cm and $\alpha_R = 89.50^\circ$, and were equivalent for all crystals analyzed. The single crystal selected for our experiment had dimensions $0.2 \times 0.2 \times 0.2$ mm³ and a mass ~ 0.05 mg.

Magnetization was measured with the SHE-330X series SQUID system with SQUID sensor installed in the vacuum chamber of the 3He / 4He dilution refrigerator. The sensor was thermally anchored to the liquid He bath (4.2 K) and shielded with a Nb tube. Two counter-wound pickup coils were connected to the input coil of the SQUID sensor. The SQUID pickup coils were placed in the center of a 10 cm long superconducting solenoid generating a magnetic field up to 1.5 kOe. Both the coils and the solenoid were fixed to the mixing chamber of the dilution refrigerator. Details of the experimental setup are described elsewhere.¹⁸ The perfect shielding ($4\pi M = -H_0$) of the Meissner state was used to calibrate the SQUID system. The crystal was oriented with the magnetic easy axis (the [111] crystallographic triple axis) parallel to the external magnetic field. For this orientation, the demagnetizing factor was assumed to be $k = 1/3$.

EXPERIMENTAL RESULTS AND COMPARISON WITH THEORY

In Fig.2, the magnetization M measured as a function of temperature is presented for several applied magnetic fields oriented parallel to the easy axis of the single crystal. At higher temperatures, the transition to the super-

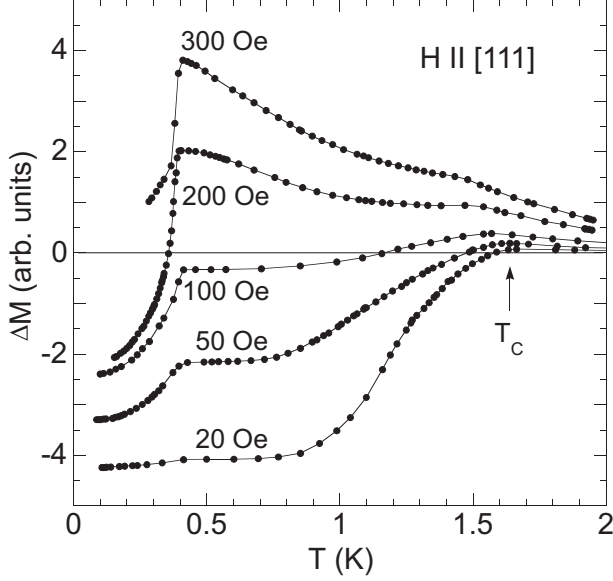


FIG. 2: Magnetization versus temperature at several applied fields for DyMgS_8 single crystal for the field direction oriented parallel to the magnetic easy axis.

conducting state is observed at T_c as the smooth decrease of M (e.g., $T_c = 1.62$ K for $H_0 = 20$ Oe). This critical temperature is clearly field dependent as expected for a superconductor. At low fields, M reaches negative values close to T_c . At higher fields, this is not possible because of the induced strong paramagnetic moment of the Dy ions. At low temperatures, the abrupt change of M is observed at $T_N = 0.4$ K, reflecting the transition to the AF state. In that state, the internal field is reduced and M can now become negative even for higher fields. At T_N and for $H_0 = 200$ Oe, the change of M between the paramagnetic (PM) and AF states increases significantly with increasing field, as expected. However, for $H_0 > 200$ Oe, the single crystal is in the SF phase^{19,20} and the observed change of M , caused by the transition to the ordered state, now decreases with increasing field. The low-field part of the $B(H_0)$ virgin curve is presented in Fig.3 to show the details of flux penetration. This penetration is typical above $T_N = 0.4$ K and proceeds as an unusual two-stage process at lower temperatures where AF order coexists with superconductivity. At low fields the sample is in the Meissner state. When the field increases above $H_{en1} = 60$ Oe (90 Oe, after correction for demagnetizing effects) the sample is penetrated by the flux. Then, at higher fields, the penetration process stops unexpectedly and B is constant in the sample while

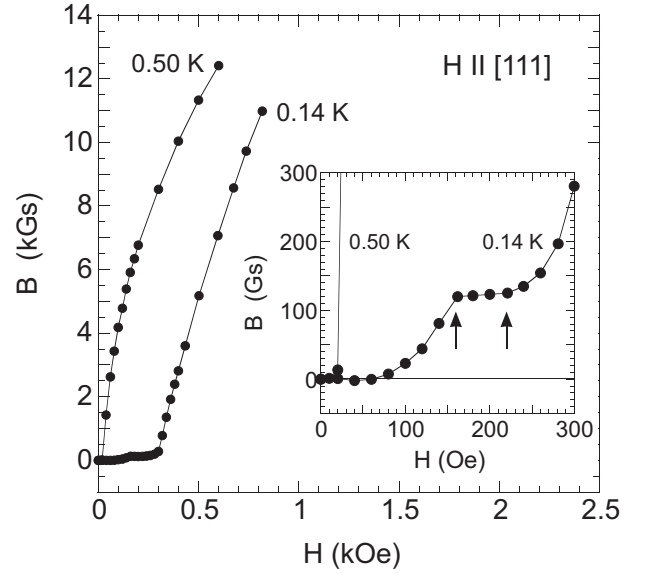


FIG. 3: Magnetic induction for DyMgS_8 single crystal in the virgin state measured as a function of an applied field at temperatures above and below $T_N = 0.4$ K. The field direction is oriented parallel to the magnetic easy axis of the crystal. The inset shows the details of the magnetization process at low fields. The arrows show the external fields for which the magnetic flux first stops then begins to penetrate into the sample again. The results are not corrected for demagnetizing effects (see text).

the external field is further increased. This new perfect shielding appears at $H_0 = 160$ Oe (180 Oe, after correction for demagnetizing effects). The penetration process starts again when the external field reaches $H_0 = 220$ Oe (270 Oe, after correction for demagnetizing effects). This value we call the second critical field for flux penetration $H_{en2}(B)$.

In order to compare our calculations with the experimental results, it is necessary to estimate several quantities. The most important one is the Ginzburg-Landau (GL) parameter κ . We have calculated for our sample to be 2.5. The method of calculation of κ from the experimental data in the case of the antiferromagnetic superconductor is presented elsewhere.¹⁸

To find the thermodynamic critical field H_T and then to calculate $H_{en2}(B)$ we propose the following argumentation. At low fields, in the vicinity of the lower critical field H_{c1} , the intensity of the field in the vortex core is $2H_{c1}$.²¹ When the external field is increased the field intensity in the vortex core increases because of the superposition of the fields of the surrounding vortices. Taking into account only the nearest neighbors we can write

$$H_T = 2H_{c1} + z \frac{H_0}{2} K_0 \frac{d}{\lambda}, \quad (24)$$

where for H_{c1} we put the value of $H_{en1} = 90$ Oe, as it is usually done, and d denotes intervortex spacing. The number of the nearest vortices is denoted by

z , and $d =$ corresponds to that value of B for which the penetration process unexpectedly stops. In Fig.3, this value is easily seen to be $B = 120$ G. The relations $B = 2'_{\phi} d^2 \sqrt{3}$ (for triangular lattice of vortices), $'_{\phi} = 2 H_{c2}^2$, ($H_{c2} = 900$ Oe at $T = 0.14$ K), enable us to obtain $d = 2.95$. This value, inserted into Eq.(24) gives $H_T = 210$ Oe. Taking into account the volume of the elementary cell of DyMgO_6S_8 , $V = 268 \cdot 10^{24} \text{ cm}^3$, we can estimate the saturation magnetization of Dy ions $8 M_0 = 3780$ G. Then, we use Eq.(6) to calculate M in the SF-phase domain

$$M = 2M_0 \cos \theta = \frac{2KM_0^2}{H_T}. \quad (25)$$

The anisotropy coefficient $K = 0.442$ was determined by finding the best fit of the theoretical with the experimental magnetization curves.²⁵ This coefficient inserted into Eq.(25) gives the magnetization in SF domain $4 M = 1200$ G, corresponding to the external field $H_0 = 180$ Oe for which penetration stops. Finally, inserting all the above values into Eqs.(22,23) we have obtained $H_{en2}(B) = 310$ Oe, which is in excellent agreement with the value observed in the experiment $H_{en2} = 270$ Oe. In our calculations we have underestimated the value of M in Eq.(25) assuming in Eq.(8) constant magnetization across the SF domain, equal to its value at the boundary between AF and SF phases. The real magnetization in SF domain is increasing toward the center of the vortex. One can easily check that higher value of M would give slightly lower value of $H_{en2}(B)$.

Conclusion

We have demonstrated that the antiferromagnetic superconductor DyMgO_6S_8 shows very interesting behavior in the magnetic field applied below T_N . When the sample is in the virgin state, initially it magnetizes like ordinary type II superconductor. Upon the applied magnetic

field of intensity equal to the critical field for flux penetration the sample undergoes the transformation from the Meissner to the mixed state. Then, magnetization proceeds in an unusual way. When the field is further increased a new state appears, a kind of a Meissner state but, in the contrary to the previous one, with a constant flux density in the sample. Characteristic plateau on the magnetization curve, shown in the inset of Fig.3, proves that magnetic flux density inside DyMgO_6S_8 is unaffected by the increased external field. If the applied field reaches certain value of intensity, we call it second critical field for flux penetration, the flux starts to enter into the sample again. This phenomenon we name two-step flux penetration. We have assumed that in this new Meissner-like state vortices undergo metamorphosis to the shape shown in Fig.1. During that process a domain of spin-op phase is created around the vortex core. That metamorphosis leads to a spatial redistribution of the shielding supercurrent flowing around the core so as to keep constant the flux carried by the vortex and, also, leads to a redistribution of the magnetic induction inside the vortex. Finally, a new energy barrier is formed near the surface preventing vortices from entering into the sample. In effect the number of vortices is kept constant inside the superconductor, hence the magnetic induction is constant. To overcome this barrier by the vortices with the newly created magnetic structure the external field must be increased beyond the second critical field for flux penetration. Using the image method we have calculated this field. The calculated value is in an excellent agreement with the measured one.

Acknowledgments

We would like to thank Professors J. Sznajd and T. Kopec for helpful discussions. This work supported the State Committee for Scientific Research (KBN) within the Project No. 2 P 03B 125 19.

- ¹ For review see Superconductivity in Ternary Compounds, edited by M. B. Maple, and F. Fischer, Springer-Verlag, Berlin, 1982.
- ² L. N. Bulaeviskii, A. I. Buzdin, M. Kulic and S. V. Panjukov, Advances in Physics 34, 176 (1985), Sov. Phys. Uspekhi 27, 927 (1984).
- ³ M. B. Maple, Physica B 215, 110 (1995).
- ⁴ L. Bauernfeind, W. W. Idler, and H. F. Braun, Physica C 254, 151 (1995).
- ⁵ I. Felner, U. Asaf, Y. Levi, and O. Millo, Phys. Rev. B 55, R3374 (1997).
- ⁶ I. Felner, U. Asaf, S. Reich, and Y. T. Sabba, Physica C 311, 163 (1999).
- ⁷ C. Bernhard, J. L. Tallon, Ch. Niedermayer, Th. Blasius, A. Golnik, E. Brcher, R. K. Kremer, D. R. Noakes, C. E. Sronach, and E. J. Ansaldo, Phys. Rev. B 59, 14099

- (1999).
- ⁸ D. J. P. Pringle, J. L. Tallon, B. G. Walker, and H. J. Trodahl, Phys. Rev. B 59, R11679 (1999).
- ⁹ A. Fainstein, E. Winkler, A. Butera, and J. Tallon, Phys. Rev. B 60, R12597 (1999).
- ¹⁰ M. Houzet, A. I. Buzdin, and M. Kulic, <http://arxiv.org/abs/cond-mat/0105480>.
- ¹¹ S. S. Saxena, P. Agarwal, K. Ahilan, F. M. Grosche, R. K. W. Haselwimmer, M. J. Steiner, E. Pugh, I. R. Walker, S. R. Julian, P. Monthoux, G. G. Lonzarich, A. Huxley, I. Sheikin, D. Braithwaite, and J. Flouquet, Nature 406, 587 (2000).
- ¹² C. P. Eiderer, M. Uhlir, S. M. Hayden, R. Vollmer, H. v. Lohneysen, N. R. Bernhoeft, and G. G. Lonzarich, Nature 412, 58 (2001).
- ¹³ N. K. Sato, N. Aso, K. Miyake, R. Shiina, P. Thalmeier,

- G. Varelogiannis, C. Geibel, F. Steglich, P. Fulde, and T. Komatsubara, *Nature* 410, 340 (2001).
- ¹⁴ T. K rzyszto n, *J. Mag. Mag. Mater.* 15-18, 1572 (1980).
 - ¹⁵ T. K rzyszto n, *Phys. Letters A* 104, 225 (1984).
 - ¹⁶ A. I. Buzdin, S. S. K rotov, and D. A. K uptsov, *Solid State Comm un.* 75, 229 (1990).
 - ¹⁷ H. Iwasaki, M. Ikebe and, Y. M uto, *Phys. Rev. B* 33, 4669 (1986).
 - ¹⁸ K. Rogacki, E. T jukano , and S. Jaakkola, *Phys. Rev. B* 64, 094520 (2001).
 - ¹⁹ W. Thom linson, G. Shirane, D. E. M oncton, M. Ishikawa and, . Fischer, *J. Appl. Phys.* 50, 1981 (1979).
 - ²⁰ W. Thom linson, G. Shirane, J. W. Lynn, and D. E. M oncton, in *Superconductivity in Ternary Compounds*, edited by M. B. M aple, and . Fischer, Springer-Verlag, Berlin 1982.
 - ²¹ M. T inkham , *Introduction to Superconductivity*, chapter 5, M cG raw-H ill Inc., New York 1975.
 - ²² J. R. C lem , in *Proceedings of the 13th Conference on Low Temperature Physics (LT 13)*, vol. 3, P lenum -P ress, New York 1974, p. 102.
 - ²³ T. K rzyszto n, G. K ozlowski, and P. Tekiel, *Acta Phys. Polon, A* 56, 49 (1979).
 - ²⁴ R. H ory n, O. Pena, C. Geantet, and M. Sergent, *Supercond. Sci. Technol.* 2, 71 (1989).
 - ²⁵ A. H. M orrish, *The Physical Principles of Magnetism*, chapter 6, John W iley and Sons, Inc. New York 1965.